Optical Materials 140 (2023) 113780

Contents lists available at ScienceDirect

Optical Materials

journal homepage: www.elsevier.com/locate/optmat

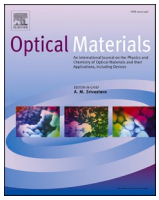

Research Article

Improving the current density and reducing the recombination rate of dye sensitized solar cells by modifying the band gap of Titania using Novel heterostructures

M.I. Khan [a,**], Shazia Mumtaz [a], Ghulam M. Mustafa [b,*], Mongi Amami [c], Urram Shahzad [a], Eman A. Al-Abbad [d,e]

[a] Department of Physics, The University of Lahore, 53700, Pakistan
[b] Department of Physics, Division of Science and Technology, University of Education, Lahore, Punjab, 54770, Pakistan
[c] Department of Chemistry College of Sciences, King Khalid University, P.O. Box 9004, Abha, Saudi Arabia
[d] Department of Chemistry, College of Science, Imam Abdulrahman Bin Faisal University, P.O. Box 1982, Dammam, 31441, Saudi Arabia
[e] Basic and Applied Scientific Research Centre, College of science, Imam Abdulrahman Bin Faisal University, P.O. Box 1982, Dammam, 31441, Saudi Arabia

ARTICLE INFO

Keywords:
Dye-sensitized solar cells
TiO_2
Cd
Doping

ABSTRACT

Here we report the synthesis of thin films of pristine TiO_2, 1% Cd-doped TiO_2 (Cd–TiO_2), TO_2/Cd–TiO_2, and Cd–TiO_2/TiO_2 on FTO glass substrates using the sol-gel dip-coating method. XRD shows that all films have an anatase crystal phase. The maximum intensity and large grain size (48.89 nm) in a 1% Cd–TiO_2/TiO_2 bilayer film have been observed. Detailed optical properties like absorbance, transmittance, band gap energy (E_g), refractive index (n), dielectric constant, and extinction coefficient (k) have been calculated by UV–Vis. Spectroscopy. According to UV–Vis results, all films absorb UV radiation and transmit visible radiation. The film of 1% Cd–TiO_2/TiO_2 is a good electrode for solar cell applications due to its low E_g (2.9 eV) and strong transmittance in the visible region. The dye-sensitized solar cells (DSSCs) of these films have been prepared with N719 dye. The cell made up of 1% Cd–TiO_2/TiO_2 photoanode has the maximum power conversion efficiency (2.47%) in comparison with a pure TiO_2 photoanode (1.32%) due to an improvement in the transfer of electrons from the LUMO of dye to the conduction band of TiO_2.

1. Introduction

Just two decades ago, in 1999, consumption rate of energy in the world was 12.7 TW. But in 2050, almost 46% more energy (26.4 TW) will be required. The demand for electricity in daily life is increasing day by day. Therefore, it would become 58.7 TW [1]. The usage of fossil fuels in every sector of daily life, especially those related to energy, is increasing daily. Approximately 70% of energy-based devices directly or indirectly depend upon fossil fuels. The earth's temperature is rising by 0.5–1.1 °F a year; therefore, the usage of these fossil fuels, which is also to blame for flooding, ozone depletion, and global warming [2]. Consequently, the importance of renewable power sources has increased in the quest for fossil fuel independence. The most suitable way to resolve the global energy disaster is to utilize solar energy as renewable energy. The main technologies that convert sunlight into electricity are solar cells. Among different solar cells, dye-sensitized solar cell (DSSC) is suitable because of their amazing properties like simple manufacturing process, low cost, elasticity, environmentally friendly, and high efficiency [3,4]. Theoretically, a maximum of 30% efficiency can be achieved by a DSSC [5], but experimentally, 14.3% has been achieved [4,6]. Dyes, electrolytes, semiconductor photoanodes, and counter electrodes are the main components of DSSC. The photoanode is an important component of dye loading and electron transmission from the dye molecule to the external circuit [7]. The photoanode substance titanium dioxide (TiO_2) is frequently utilized in present days due to its non-pollutant nature, large surface area, and high energy conversion efficiency [8]. The fundamental constraint associated with employing TiO_2 as a photoanode is irregular electron transportation, which is responsible for electron-hole recombination and lower cell efficiency [9]. Constructing photoanodes with an effective charge transfer channel

* Corresponding author.
** Corresponding author.
E-mail addresses: Muhammad.iftikhar@phys.uol.edu.pk (M.I. Khan), dr.ghulam.muhammad@ue.edu.pk (G.M. Mustafa).

https://doi.org/10.1016/j.optmat.2023.113780
Received 10 February 2023; Received in revised form 3 April 2023; Accepted 7 April 2023

may overcome this issue. TiO_2 film surface changes via doping are a hot issue for this reason. Several elements like Ce, In, Cd, Fe, or Cr are used for doping purposes in TiO_2 [10]. Among all these metals, Cd is the best material for doping in TiO_2 because Cd increases dye absorption and electron injection efficacy rate from the lowest unoccupied molecular orbit (LUMO) of dye to the conduction band (CB) of TiO_2 [11,12]. It was observed that 1% Cd doping in TiO_2 resulted in strong catalytic behavior [12].

Like doping, bilayers also increase the current density and decrease the recombination rate. In different layers, the Fermi level is aligned, which improves the efficiency of the cell [13]. As a result, the bilayer technique is ideal for improving photovoltaic performance [4,14]. Therefore, for high-performance DSSCs, an alternate layer of 1% Cd–TiO_2 and TiO_2 films was synthesized in the current study. The injection efficiency rate of electrons has been improved by Cd doping from dye to the CB of TiO_2. The role of bilayers consists of blocking electrons leakage could be possible by alternating layers concept from FTO to oxidized electrolyte mediator. Thus, this doping and bilayer will enhance the photovoltaic parameters of the cell. From the literature survey, it is found that the work on doping and multilayer is very limited and needs further investigation to check their suitability for DSSC applications [15]. Flow of electrons through the different layers of cell is shown in Fig. 1.

2. Experimentation

This study include the synthesis of thin films of pure TiO_2, 1% Cd–TiO_2, TiO_2/1% Cd–TiO_2, and 1% Cd–TiO_2/TiO_2 were deposited on FTO glass substrate using sol-gel assisted dip-coating method. Initial cleaning of FTO slides was performed in an ultrasonically for a short period, followed by DI water and acetone washing and drying. From Sigma-Aldrich, cadmium acetate (Cd $(OAC)_2$), Ti $[OCH\ (CH_3)_2]_4$ (titanium (IV) isopropoxide), acetone, ethanol, N719 dye (ruthenium dye), and methanol were bought. 23 ml of ethanol and 23 ml of titanium isopropoxide were dissolved at constant stirring to get a TiO_2 solution. After that, 24 mL of DI H_2O was added to the mixture. That is solution A. A magnetic stirrer was used to stir this combination constantly until the gel was achieved. For a 1% Cd–TiO_2 solution, identical steps are used to create solution A. After adding 1% Cd $(OAC)_2$ to solution A, the mixture was continually agitated till the gel was achieved. These solutions aged for a total of 19 h. Four FTO substrates that had been chemically cleaned were taken. A single piece was submerged in the TiO_2 mixture and dried for 12 min at 110 °C. Afterward, it was once more submerged in TiO_2 solution and dried for 12 min at 110 °C. Two more times were spent doing the process. The same process was used to deposit a layer that included 1% Cd–TiO_2. For the purpose of depositing the TiO_2/1% Cd–TiO_2 layer, the FTO substrate was submerged twice in the TiO_2 solution and then twice in the 1% Cd–TiO_2 solution to achieve an identical thickness. The same process was used to deposit a layer that contained 1% Cd–TiO_2/TiO_2. All four kinds of films underwent a 2-h annealing process in the furnace at 470 °C.

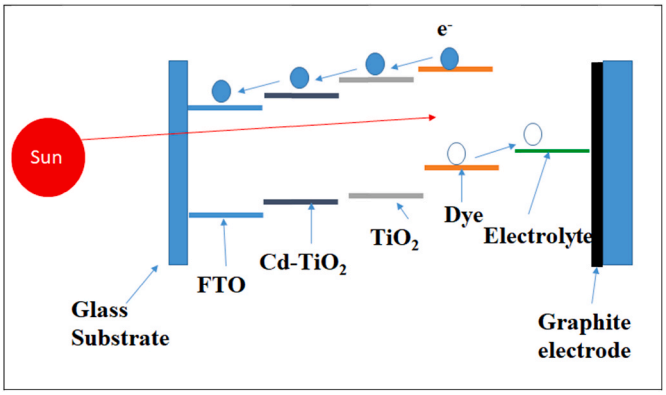

Fig. 1. Flow of electrons through the different layers of cell.

The structure of the produced films was explained using an X-ray diffractometer (PANalytical, D/Max-III). SEM images were measured by (FEI Sirion). By UV–Visible spectrophotometry (HITACHI U-2800), optical properties were measured.

These films were dipped in a dye (N719) solution for 23 h in order to fabricate solar cells. These are photoanodes. The counter electrodes (CEs) were formed by graphite coating on FTO-glass substrates. Both the photoanode and the CE were sealed. A tiny hole was drilled into the CEs to deliver a liquid iodide/tri-iodide electrolyte, and another hole was used to draw air. Using solar simulator, the IV characteristics were measured.

3. Results and discussion

3.1. XRD analysis

Fig. 2(a) showed the XRD pattern of TiO_2, 1% Cd-doped TiO_2, and bilayer films. The films' whole diffraction peak matching with PDF # 21–1272 demonstrated the anatase phase's tetragonal structure [16]. TiO_2 film-related peaks in the XRD results were seen at 2θ values of 25.28°, 37.84°, 48.05°, and 62.68°. Because certain peaks have more regularity than others, they have higher intensities [4]. Due to a larger electron density variation, more intense peaks are seen at 2θ values 25.25°, 37.80°, 48.045°, and 62.62° at 1% Cd–TiO_2 film. That suggests that 1% Cd-doping enhanced the crystalline nature of the film. Due to the 1% Cd-doping, some red shift in the peaks has been seen. Ti (0.605 Å) [17] and Cd (0.950 Å) [18] have different ionic radii, which causes the peaks to shift. Additionally, it is noted that after Cd doping, there is no additional peak of Cd–Ti, CdO, etc., indicating that Cd ions have been fully incorporated into TiO_2. Due to the inclusion of Cd in the TiO_2 lattice, Cd–Ti–O was efficiently partially transformed from Cd^{2+} and Ti^{4+} [19]. The greatest increase in peak intensity is seen when the TiO_2 layer is placed onto Cd–TiO_2 film. Because of the rise in crystallinity, this film is suitable for use in applications involving solar cells [20]. The absence of an intermediate phase indicates that the interfacial connection between the two layers is very strong [4]. A decline in the intensity of the peak was noticed after alternating layers, such as a 1%Cd–TiO2 layer, were applied to TiO2 film, indicating that the film's crystallinity had diminished [21]. This bilayer scheme exhibited more significant intensity than single-layer films, referred that such films are suitable for solar cell applications.

Equations (1) and (2) determine the grain size (D) and defects (δ) of the highly intense peak (101) inside the crystalline structure of undoped, and doped films [22].

$$D = \frac{k\lambda}{\beta \cos \theta} \tag{1}$$

$$\delta = \frac{1}{D^2} \tag{2}$$

The boundary of a grain is called the grain boundary. For dislocation absorbance, every grain boundary has a distinct activation energy [23]. The larger the grain size, the more atoms will be trapped by the grain boundary [4,24]. Large particle sizes reduce the surface area, which is responsible for strong light scattering, and small particle sizes with large surface areas result in a weak light-scattering effect [25]. TiO_2 film has 18.3 nm of D and $2.69 \times 10^{15}\ m^{-2}$ of δ. By doping TiO_2 film with 1% Cd, its D reached 20.4 nm and δ became $2.32 \times 10^{15}\ m^{-2}$.

This shows that the Cd doping has lowered the charge recombination rate while increasing the crystallinity of the TiO_2 layer [26]. The 1% Cd–TiO_2/TiO_2 films have a small irregularity and a large grain size ($0.520 \times 10^{15}\ m^{-2}$ and 43.7 nm) in comparison with TiO_2/1% Cd–TiO_2 film (25.3 nm, $1.56 \times 10^{15}\ m^{-2}$). As 1%Cd–$TiO_2$ has a large grain size than TiO_2 film. Therefore, this is responsible for a larger grain size of 1%

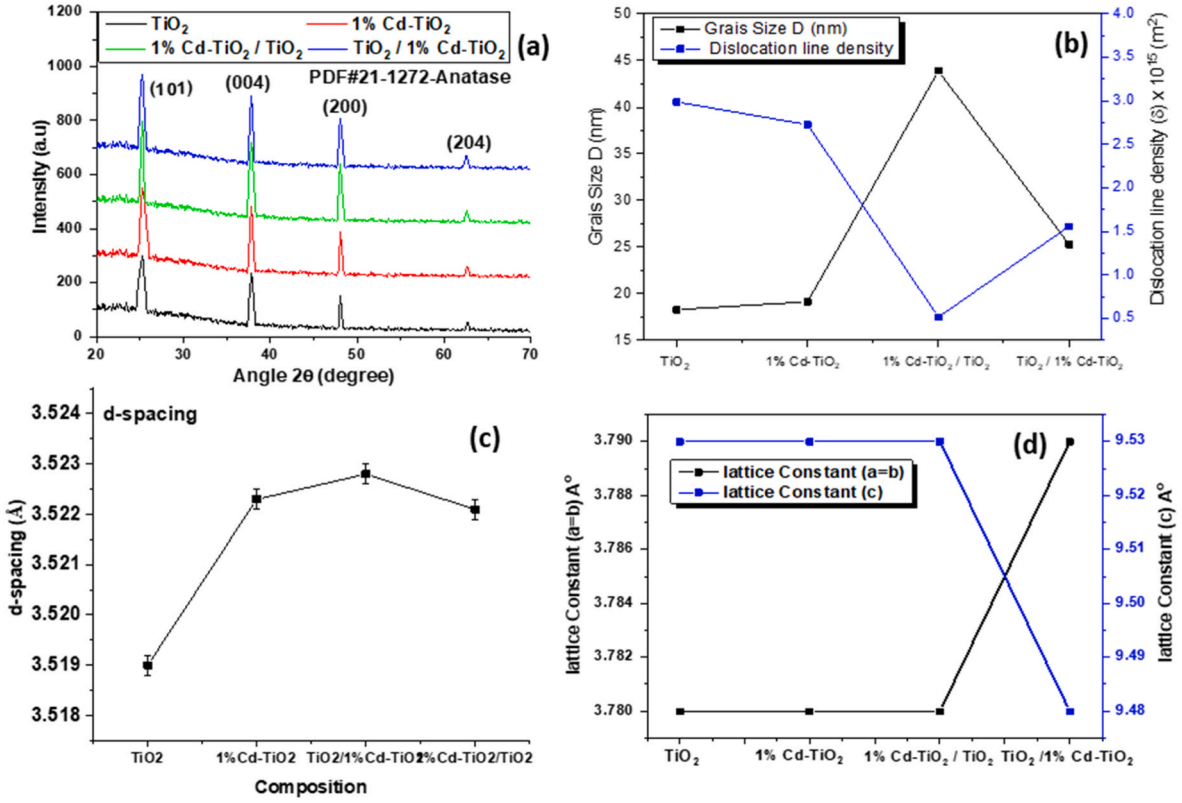

Fig. 2. **(a)** XRD patters, (b) grain size and dislocation line densit, (c) d-spacing and (d) lattice parameters of deposited films.

Cd–TiO_2/TiO_2 films [4]. Also, these different layers will affect the efficiency of DSSCs. The underlayer plays a more important role than the top layer because the large particle size in the bottom layer recaptures the scattered light. The top TiO_2 layer will also increase the reabsorption. Thus, for getting higher efficiency, 1%Cd–TiO_2 layer at the bottom and small particle size TiO_2 layer at top is the best combination [27]. In Fig. 2(b) and Table 1, respectively, are plotted and enumerated the computed values δ of and D.

The d-spacing for all compositions was calculated using Bragg's law [28] and obtained value is provided in Table 2. Calculated and standard values are similar (PDF # 21–1272, Anatase). Very little fluctuation in d-spacing refers to the full incorporation of Cd into the TiO_2 lattice and the interstitial location.

The following expression is used to calculate the lattice parameters [28].

$$\frac{1}{d^2}=\frac{l^2}{c^2}+\frac{k^2+h^2}{a^2} \tag{4}$$

Table 2 lists the lattice parameter values for the intense (101) peak of fabricated films that are matched with PDF # 21–1272. The computed values of the d-spacing and lattice parameters are plotted in Fig. 2 (c and d).

3.2. Raman analysis

Raman spectra are used to investigate the elemental composition

Table 1
Crystallite size (D) and crystal strain (δ) of films.

Samples	D (nm)	Δ (m^{-2}) × 10^{15}
TiO_2	18.3	2.99
TiO_2/1%Cd–TiO_2	25.3	1.56
1%Cd–TiO_2	19.2	2.73
1%Cd–TiO_2/TiO_2	43.89	0.519

Table 2
d-spacing and lattice constant values.

Sample	lattice constant (Å)	d-spacing (Å)
TiO_2	c = 9.53, a = 3.78	3.52 Å
1%Cd–TiO_2/TiO_2	c = 9.53, a = 3.78	3.52 Å
1%Cd–TiO_2	c = 9.53, a = 3.78	3.52 Å
TiO_2/1%Cd–TiO_2	c = 9.48, a = 3.79	3.52 Å

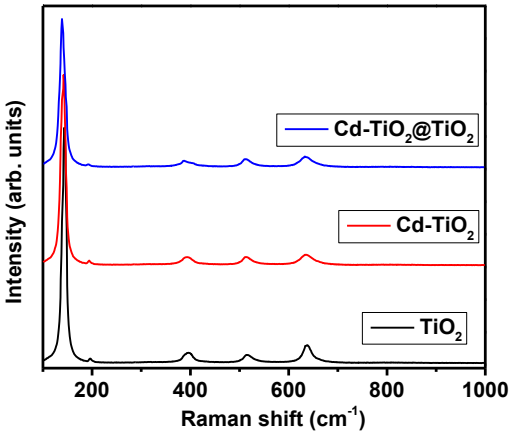

Fig. 3. Raman spectra of deposited films.

further. The spectra of films are shown in Fig. 3. The structure of the TiO_2 crystal was investigated using Raman analysis. Six active modes of Raman, at 639 cm^{-1} (E_g), 519 cm^{-1} (superimposed with the 515 cm^{-1} bands) (A_{1g}, B_{1g}), 399 cm^{-1} (B_{1g}), 197 cm^{-1} (E_g), and 144 cm^{-1} (E_g), are well-known to exist in anatase. The five active Raman modes in the rutile phase, however, are at 826 cm^{-1} (B_{2g}), 612 cm^{-1} (A_{1g}), 447 cm^{-1} (E_g), 240 cm^{-1} (multi-photon process), and 143 cm^{-1} (B_{1g}). Unusual for TiO_2, a peak at 685 cm^{-1} is linked to the heat treatment and embedded CdNPs. The predominant TiO_2 coating in the modes of Raman spectra can be attributed to the active modes of Raman in the anatase phase at wavelengths of around 637 cm^{-1} (Eg(3)), 514 cm^{-1} (A1g, B1g(2)), 395 cm^{-1} (B1g(1)), 197 cm^{-1} (Eg(2)), and 144 cm^{-1} (Eg(1)) [21]. The quantum size effect may be to blame for the lack of Cd peaks [20].

3.3. SEM analysis

The SEM images of pure TiO_2, 1% Cd–TiO_2/TiO_2 are presented in Fig. 4 (a and b). It is obvious from these images that pure TiO_2 shows a porous morphology with very small pours at the surface. TiO_2 is a popular material for solar cell electrodes due to its unique properties, such as high transparency, inexpensive, chemically stable, and n-type semiconducting behavior. Porous morphology is crucial for the effective operation of solar cell electrodes because it offers a significant contact area for photon absorption and electron transfer, which increases the efficacy of cell [29]. 1% Cd–TiO_2/TiO_2 shows that porosity is increased also the film is smooth and no racks inside it. Therefore, it will adsorb more dye and also it prevent the electrode to reach to the FTO interface due to fully covered 1% Cd–TiO_2/TiO_2. This will avoid the short circuit with in the cell. Also, 1% Cd–TiO_2/TiO_2 is supposed to narrow the bandgap than pure TiO_2, which allows it to take in more of the solar spectrum [30]. Additionally, Cd-doped TiO2 will facilitate the electron transport properties because of the existence of the vacancies of Cd that serve as electron donors.

3.4. Optical properties

By recording the UV–visible absorption spectra, properties related to the optical absorption of TiO_2, 1%Cd–TiO_2 films & bilayer films are investigated (Fig. 5(a)). It is observed that all absorbance peaks have sharp cut-offs at 350–400 UV wavelength, which means the maximum UV region of light has been absorbed, and electrons started to move from HOMO to LOMO levels at this wavelength range [31]. The absorbance of the Cd–TiO_2/TiO_2 film was higher than that of other films. In all doped and bilayer films, redshift is observed, indicating a reduction in bandgap [4]. The large absorbance in the UV region and maximum shift towards a longer wavelength of the 1%Cd–TiO_2/TiO_2 film indicate that the combination of the two layers is good for solar cell applications [19,26].

The band-gap energy (E_g) values of the deposited films were calculated using Tauc plot method and is given below [32].

$$(\alpha h\nu) = A\left(h\nu - E_g\right)^z \tag{5}$$

The graph between E (hν) and $(\alpha h\nu)^{1/2}$ in eV was beneficial to determine E_g. A is a constant, and the electronic transition nature is represented by the exponent (z). For indirect and direct band gaps, z = 2, z = 1/2, respectively [33]. Results show that z = 1/2 is very suitable for getting a more genuine and well-founded plot [34].

The value of the absorption coefficient (α) was determined using the equation below [35]

$$\alpha = \frac{2.303A}{t} \tag{6}$$

In Equation (6), 'A' is the absorbance, and 't' is the thickness of the film. From the steep portion, by extrapolating along the x-axis, the E_g value is calculated. Calculated E_g values of TiO_2, 1%Cd–TiO_2/TiO_2, 1%Cd–TiO_2, and TiO_2/1%Cd–TiO_2 bilayer films are 3.19, 2.9, 3.05, and 3.01 eV, respectively (Fig. 5(b)). At Cd doping, a reduction in E_g (3.05 eV) value is observed. Due to free-electron properties, there is downward and upward shifting in the conduction band (CB) and valence band (VB), respectively, which is responsible for the reduction in the E_g value [4,36], due to the interchange of oxygen 2p states with Cd 2p states in the TiO_2 lattice [37]. The charge recombination process is very helpful for understanding the mechanism of DSSCs and their photoelectrochemical features. The Cd–TiO_2/TiO_2 film has a small E_g (2.9 eV) value. Shifting of E_g towards a lower value due to Cd doping was observed because Cd launched inters band energy levels in TiO_2 film bandgap [38].

The fabricated Cd–TiO_2/TiO_2 film has a very high transmittance value, near 80% in the visible region. In the nearby short wavelength region, the transmittance of the TiO_2 thin film was abruptly changed (Fig. 5(c)) by 1% Cd doping due to band-to-band transition. That was also due to the VB and CB absorption of excited electrons. A change in the absorption coefficient was also responsible for changes in bandgap energy values in this region [39].

$$T(\%) = \frac{1}{\exp(\alpha t)} \tag{7}$$

The transmittance pattern was increased with increasing wavelength (λ) of all deposited films, especially with 1%Cd–TiO_2/TiO_2 bilayer. Due to their excellent transmittance in the visible spectrum, such films are suitable for DSSC electrodes [40].

The extinction coefficient for deposited films vs. wavelength is shown in Fig. 6(a). Relationships can be used to compute "k" [39],

$$\kappa = \alpha\lambda/4\pi \tag{8}$$

Fig. 6(a) demonstrates that the "k" is rising with doping and bilayer. The bilayer films progressively improve the visible photon energy section. With the bilayer, this rise in "k" induced an increase in surface optical loss and optical scattering due to film thickness [41]. The

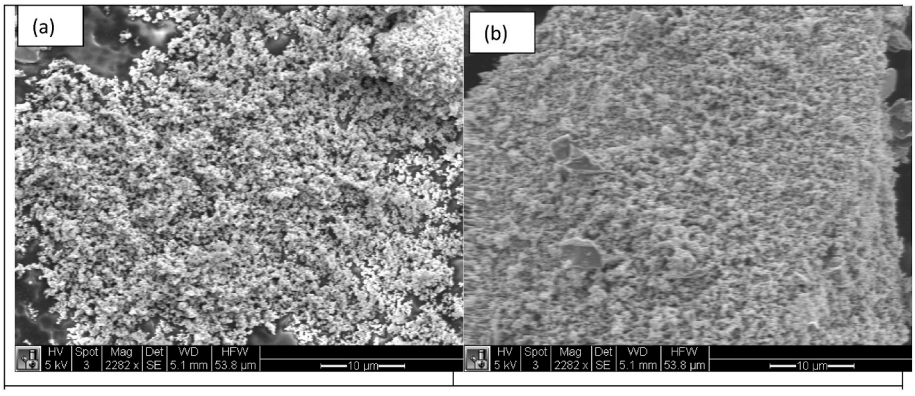

Fig. 4. SEM of (a) TiO_2 and (b) Cd–TiO_2/TiO_2.

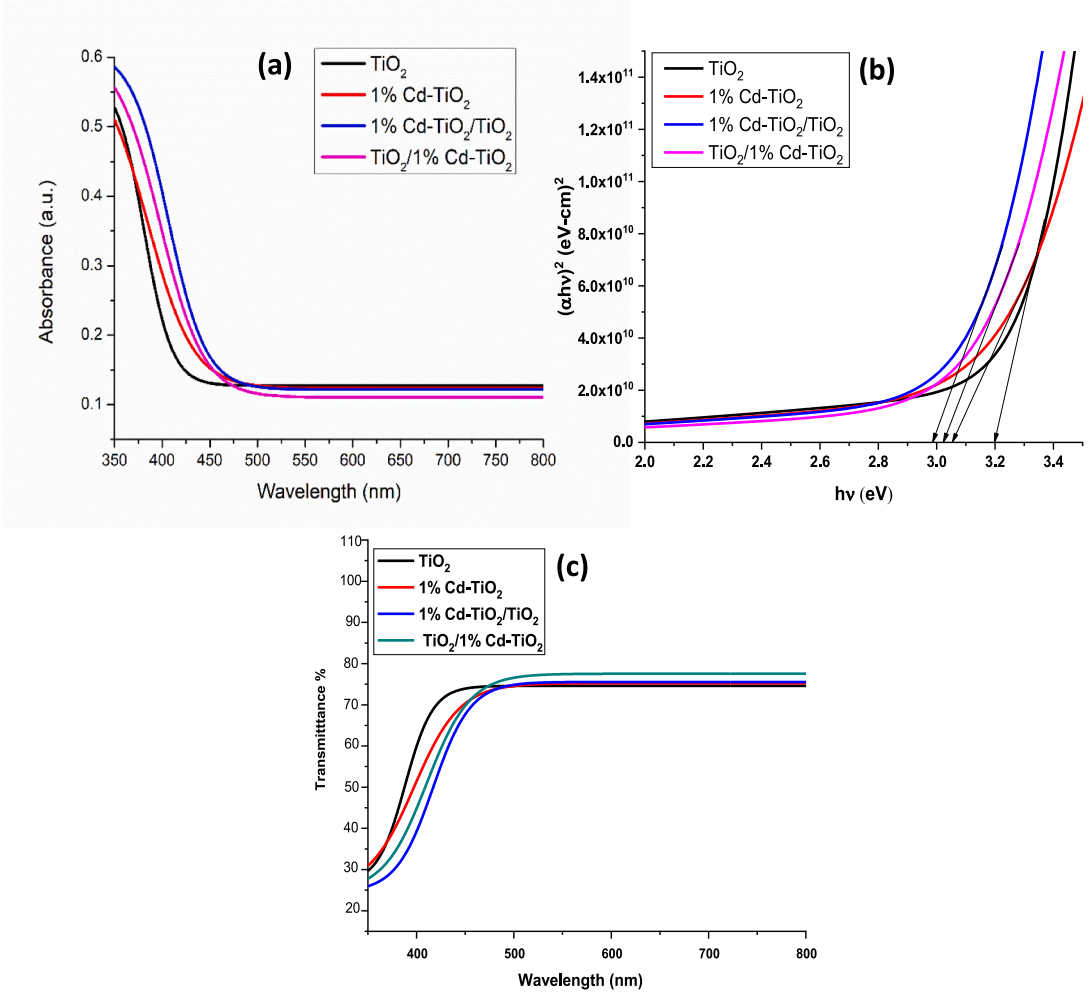

Fig. 5. (a) Absobance versus wavelength, (b) Tauc plot and (c) transmission spectra of fabricated films.

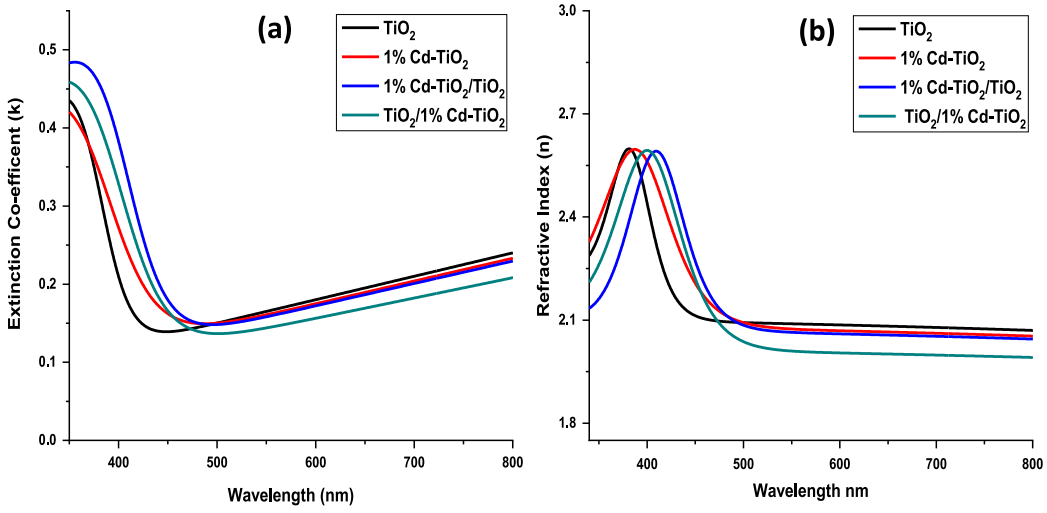

Fig. 6. (a) Extinction coefficient and (b) refractive index of fabricated films.

extinction coefficient rises in the UV range, falls as one advances to longer wavelengths, and then rises once more. For photon energy below the basic absorption edge, the "k" has a nonzero value because the increase and decrease in the "k" are directly related to the light absorption [42].

The index of refraction (n) is a fundamental property of any optical material. The primary variables on which the "n" relies in the optical material are the local field and the ion's electronic polarization. So, for the manufacturing of any optical device, the calculation of "n" is considered very important [4,41].

$$n = \left(\frac{1+R}{1-R}\right) + \sqrt{\frac{4R}{(1-R)^2} - k^2} \tag{9}$$

The function of incident light wavelength is related to the resultant of "n" (Fig. 6(b)). The "n" of TiO_2 film displays a near-visible portion of the spectrum. The value of "n" is moved towards the visible portion at 1% Cd doping. This shifting is due to the low E_g. The maximum refractive index value for Cd–TiO_2/TiO_2 film is due to improvements in the surface and crystal nature of the film [42]. Two types of zones for the refractive index are present. Firstly, if refractive index values increase with increasing wavelength due to the resonance effect of 1% Cd doping into TiO_2, it is called an anomalous dispersion zone. But if the "n" value declines with wavelength due to the effects of band levels, then it is in the normal dispersion zone [43]. The same results have been observed in many studies [4].

The complex dielectric constant with wavelength dependence is used to find the elementary electron excitation spectra. The imaginary (ε_i) and real (ε_r) components of the dielectric constant are estimated by the formulas [43].

$$\varepsilon_r = n^2 - k^2 \tag{10}$$

$$\varepsilon_i = 2nk \tag{11}$$

The wavelength-dependent ε_i and ε_r values for films are shown in (b) and (a) parts of Fig. 7, respectively. The plots of n and εr can be compared because they both have smaller values. The graph showed that the dependence of the ε_i values on the k values caused them to initially decline up to a point and then grow [44]. As a result, altering n and k changed the films' dielectric properties.

3.5. J-V measurement

The J-V characteristics of different DSSCs are shown in Fig. 8(a). Different photovoltaic parameters are shown in Table 3.

The successive equation for V_{oc} [44].

$$V_{oc} = |E_F - E_{redox}| \tag{12}$$

Where E_{redox} and E_F are the I^-/I_3^- level of energy of electrolytes and Fermi energy, respectively.

Successive equations used for efficiency and Fill Factor [45].

$$\eta = \frac{FF \times V_{oc} \times J_{sc}}{p_{in}} \tag{13}$$

$$FF = \frac{V_{max} \times I_{max}}{J_{SC} \times V_{OC}} \tag{14}$$

Where P_{in} is the input power, I_{max} and V_{max} are the maximum current and voltage, respectively. TiO_2-based DSSC has V_{oc} (0.72 V), Fill Factor (0.556), J_{sc} (3.24 $mAcm^{-2}$), and efficiency (1.32%). 1% Cd doping has an amazing impact on the J_{sc} value. It has reached 3.99 $mAcm^{-2}$; as a result, the large η is 1.55%. This increase in J_{sc} means an enhancement in the transfer of electrons from the LUMO of dye to the CB of TiO_2 [4]. Active contacts between interfaces of 1% Cd–TiO_2 film and dye are also responsible for the increment in J_{SC} [46]. Further improvements are observed in bilayer films. The interlayer and top layer of the film are crucial when examining the operation of bi-layered electrodes. Therefore, the J-V curve of anatase-based DSSCs of TiO_2/1%Cd–TiO_2 and 1% Cd–TiO_2/TiO_2 is recorded as having a light-harvesting capability improved by interlayer action because it may reflect more light towards the nano-sized anatase film. Also, it adsorbed more dyes because of different particle sizes in the top and bottom layers. This will improve the photovoltaic performance of cells [4]. Therefore, optimizing the photoanode film's structure was important for further improvement. Cd–TiO_2/TiO_2 film has high V_{oc} (0.73 V), J_{sc} (5.55 mA/cm^2), FF (0.609), developing the highest efficiency (η = 2.47%) than single-layered TiO_2 film. The scattering layer has a significant role in improving the light-harvesting efficiency. It can decrease surface states and the recombination rate of charged particles and reflect the penetrating light to the electrode [47]. The electrons are transferred to the bilayer (1% Cd–TiO_2/TiO_2) CB and collected at the charger receiver (FTO), which increases the photocurrent [48]. The J-V characteristics of the TiO_2/Cd–TiO_2 based cell were similarly very good, however the η was lower than that of the Cd–TiO_2/TiO_2 film-based DSSC [49]. Literature shows that an anatase material with a large chemical capacitance and a small resistivity value also has a low recombination rate. In bilayer film, no phase change is observed; therefore, the 1% Cd–TiO_2/TiO_2 Anatase film has a large value of conduction electrons and a small value of surface reactivity than TiO_2 film [50].

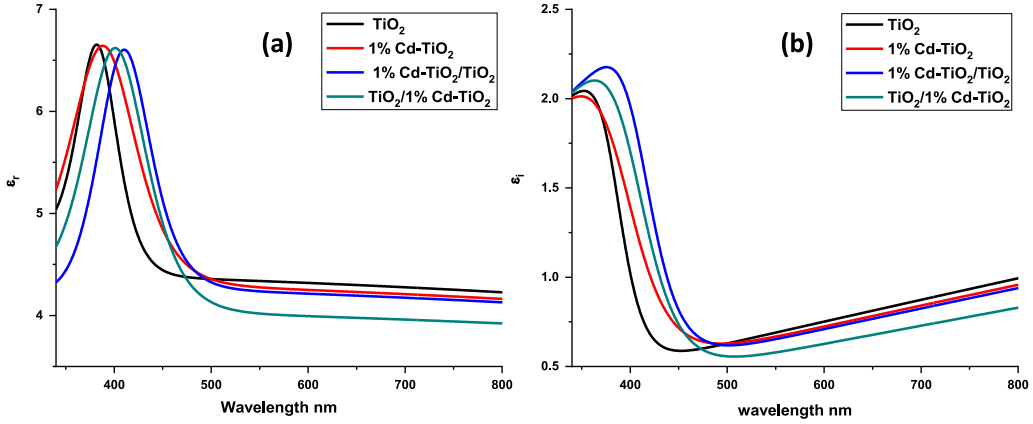

Fig. 7. (a) real parts and (b) imaginary parts of dielectric constant of fabricated films.

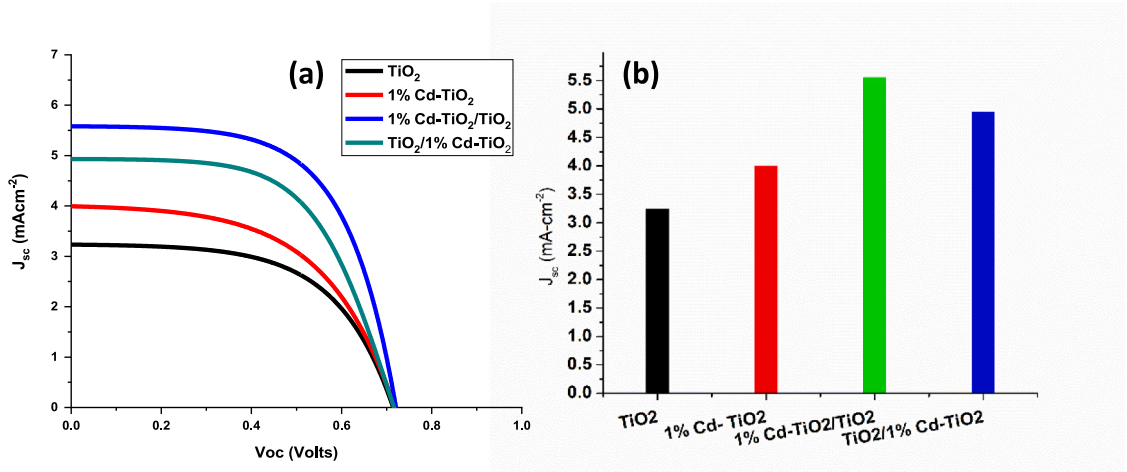

Fig. 8. (a) J-V graph and (b) Jsc of prepared cells.

Table 3
Photovoltaic parameters of cels

Samples	V_{oc} (V)	FF	J_{sc} mA/cm^2	Efficiency η%
TiO_2	0.72	0.556	3.24	1.32
TiO_2/1% Cd–TiO_2	0.72	0.590	4.95	2.105
1% Cd–TiO_2	0.72	0.557	3.99	1.55
1% Cd–TiO_2/TiO_2	0.73	0.609	5.55	2.47

Transfer electron's efficiency, scattering of light, and dye adsorption efficiency all have an effect on J_{sc} [51–53]. Under conditions of 1000 W/cm^2 of light intensity (AM 1.5 G spectrum at 25 °C), the J_{sc} of TiO_2 is around 3.24 mA/cm^2. Because Cd is an efficient electron metal and possesses unbound electrons in its outermost shell, an enhancement in J_{sc} is seen when Cd is doped in TiO_2 (Fig. 8(b)). A small quantity of energy will be lost, and these liberated electrons of Cd will impact the atoms of TiO_2, improving the J_{sc} of the DSSC (i.e., 3.99 mA/cm^2). A. Chaudhari and L. Patle [54] make a good point in that an increment in electron amount improves electron conductance and transport efficacy, which raises the J_{sc}. The amount of electrons rises and the resistivity reduces when Cd is doped in TiO_2 [54]. This improved conductivity and transportation of electrons led to an improvement in J_{sc} [55]. The theoretical model of electrical conductivity $\sigma = ne\mu$, where e, μ, and n denote the elementary charge, electron's mobility, and charge concentration, respectively, may be used to explain the rise in electron amount. Therefore, this enhances the electron's concentration, conductivity, and transport efficiency and hence enhances the J_{sc} [54,55]. The improvement in electron transfer efficacy from dye's LUMO to TiO_2's CB, as seen by the higher J_{sc} value, has increased the efficiency of DSSCs [56].

3.6. EIS analysis

To determine the charge transfer resistance of pure and Cd doped TiO_2, the EIS analysis of these two films was performed by plotting the Nyquist plot [57]. This Nyquist plot shown in Fig. 9 clearly demonstrate the semicircular shapes which is typical impedance behavior of any semiconducting behavior. The equivalent circuit which can be used to understand this EIS data is shown as inset. The charge transfer resistance at the interface of electrolyte/counter electrode is represented by the smaller semicircle at high frequency range (in the kHz range). The interface of electrolyte/dye/TiO2 charge transfer mechanism is shown by the large semicircle at low frequency range (10–100 Hz range) [58]. The diameter of this semicircle along horizontal axis determines the value of charge transfer resistance [59]. The diameter of semicircle of Cd–TiO_2/TiO_2 based cell is small therefore, the charge transfer resistance is small. This slight reduction in resistance is smooth the electronic transportation and make the functioning of solar cell better. These results are consistent with the J-V result where the Jsc is high.

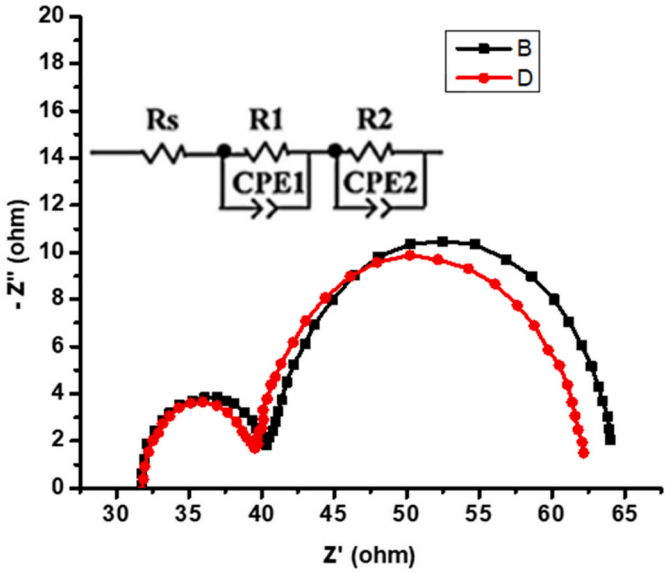

Fig. 9. Nyquist plot of pure TiO_2 and 1% Cd doped TiO_2.

4. Conclusion

Sol-gel dip coating technology has been used to successfully deposit films of TiO_2, Cd–TiO_2, and their bilayers on FTO-glass substrates. The produced films exhibit an anatase structure, according to XRD findings. The grain size of Cd–TiO_2/TiO_2 is large. UV–Vis results showed that 1% Cd–TiO_2/TiO_2 film has high transmittance in the visible area and low E_g. High values of open-circuit voltage (0.73 V), the lowest value of bandgap (2.9 eV), a large grain size (43.89 nm), small crystal defects, the high value of the refractive index, J_{sc} (5.55 mA/cm^2), FF (0.609), and the highest efficiency of about 2.47% have been achieved using 1% Cd–TiO_2/TiO_2 bilayer-based DSSCs; this composition is a potential alternative candidate for DSSCs.

CRediT authorship contribution statement

M.I. Khan: Conceptualization, Supervision. **Shazia Mumtaz:**

Writing – original draft. **Ghulam M. Mustafa:** Formal analysis. **Mongi Amami:** Facilitated in experimental equipment. **Urram Shahzad:** Facilitated in experimental equipment. **Eman Abdlrahman Al-abbad:** Final revision.

Declaration of competing interest

The authors declare that they have no known competing financial interests or personal relationships that could have appeared to influence the work reported in this paper.

Data availability

Data will be made available on request.

Acknowledgement

The authors extend their appreciation to the Deanship of Scientific Research at Kingkhalid University, Saudi Arabia for funding this work through Research Groups Program under grant number R.G.P. 2:200/44.

References

[1] A.N.B. Zulkifili, et al., The basic research on the dye-sensitized solar cells (DSSC), J. Clean Energy Tech. 3 (5) (2015) 382–387.
[2] S. Sivaranjani, Synthesis, Characterization and Application of Hetero Atom Doped Mesoporous TiO2, 2012.
[3] M. Grätzel, B. O'Regan, A low-cost, high-efficiency solar cell based on dye-sensitized colloidal TiO2 films, Nature 353 (6346) (1991) 737–740.
[4] B. Mehmood, et al., Structural and optical properties of Ti and Cu co-doped ZnO thin films for photovoltaic applications of dye sensitized solar cells, Int. J. Energy Res. (2020).
[5] K. Sharma, V. Sharma, S. Sharma, Dye-sensitized solar cells: fundamentals and current status, Nanoscale Res. Lett. 13 (1) (2018) 381.
[6] C.-P. Lee, C.-T. Li, K.-C. Ho, Use of organic materials in dye-sensitized solar cells, Mater. Today 20 (5) (2017) 267–283.
[7] M. Khan, et al., Effect of silver (Ag) ions irradiation on the structural, optical and photovoltaic properties of Mn doped TiO2 thin films based dye sensitized solar cells, Ceram. Int. (2021).
[8] H.M.A. Javed, et al., Hydrogen treated TiO2 nanoparticles onto FTO glass as photoanode for dye-sensitized solar cells with remarkably enhanced performance, Int. J. Hydrogen Energy (2021).
[9] J. Van de Lagemaat, N.-G. Park, A. Frank, Influence of electrical potential distribution, charge transport, and recombination on the photopotential and photocurrent conversion efficiency of dye-sensitized nanocrystalline TiO2 solar cells: a study by electrical impedance and optical modulation techniques, J. Phys. Chem. B 104 (9) (2000) 2044–2052.
[10] M. Okutan, et al., AC conductivity and dielectric properties of Co-doped TiO2, Phys. B Condens. Matter 364 (1–4) (2005) 300–305.
[11] M. Khan, M. Mujeeb, U. Farooq, Sol-gel deposition and electrical properties of laser irradiated Cu doped TiO2 multilayer thin films, Results Phys. 7 (2017) 2485–2488.
[12] L. Andronic, et al., Photocatalytic activity of cadmium doped TiO2 films for photocatalytic degradation of dyes, Chem. Eng. J. 152 (1) (2009) 64–71.
[13] B. Mehmood, et al., Structural and optical properties of Ti and Cu co-doped ZnO thin films for photovoltaic applications of dye sensitized solar cells, Int. J. Energy Res. 45 (2) (2021) 2445–2459.
[14] S. Pany, et al., Plasmon induced nano Au particle decorated over S, N-modified TiO2 for exceptional photocatalytic hydrogen evolution under visible light, ACS Appl. Mater. Interfaces 6 (2) (2014) 839–846.
[15] G. Fu, et al., Enhanced light harvesting in panchromatic double dye-sensitized solar cells incorporated with bilayered TiO2 thin film-based photoelectrodes, Sol. Energy 218 (2021) 346–353.
[16] L. Kavan, et al., Electron-selective layers for dye-sensitized solar cells based on TiO2 and SnO2, J. Phys. Chem. C 124 (12) (2020) 6512–6521.
[17] J. Yan, M. Greenblatt, Ionic conductivities of Bi4V2− xMxO11− x2 (M= Ti, Zr, Sn, Pb) solid solutions, Solid State Ionics 81 (3–4) (1995) 225–233.
[18] W.G. Lee, Y. Cho, S.W. Kang, Effect of ionic radius in metal nitrate on pore generation of cellulose acetate in polymer nanocomposite, Polymers 12 (4) (2020) 981.
[19] B. Naik, K. Parida, C.S. Gopinath, Facile synthesis of N-and S-incorporated nanocrystalline TiO2 and direct solar-light-driven photocatalytic activity, J. Phys. Chem. C 114 (45) (2010) 19473–19482.
[20] J. Kroon, et al., Nanocrystalline dye-sensitized solar cells having maximum performance, Prog. Photovoltaics Res. Appl. 15 (1) (2007) 1–18.
[21] T. Berger, et al., The electrochemistry of nanostructured titanium dioxide electrodes, ChemPhysChem 13 (12) (2012) 2824–2875.
[22] M. Khan, et al., Investigations of the structural, morphological and electrical properties of multilayer ZnO/TiO2 thin films, deposited by sol–gel technique, Results Phys. 6 (2016) 156–160.
[23] R.W. Siegel, G. Thomas, Grain boundaries in nanophase materials, Ultramicroscopy 40 (3) (1992) 376–384.
[24] C. Carlton, P. Ferreira, What is behind the inverse Hall–Petch effect in nanocrystalline materials? Acta Mater. 55 (11) (2007) 3749–3756.
[25] S. Mathew, et al., Dye-sensitized solar cells with 13% efficiency achieved through the molecular engineering of porphyrin sensitizers, Nat. Chem. 6 (3) (2014) 242–247.
[26] P. Nbelayim, et al., Systematic characterization of the effect of Ag@ TiO 2 nanoparticles on the performance of plasmonic dye-sensitized solar cells, Sci. Rep. 7 (1) (2017) 1–12.
[27] K. Kalyanasundaram, M. Grätzel, Applications of functionalized transition metal complexes in photonic and optoelectronic devices, Coord. Chem. Rev. 177 (1) (1998) 347–414.
[28] M. Yilmaz, G. Turgut, Titanium doping effect on the characteristic properties of sol-gel deposited ZnO thin films, Kovove Mater. 53 (2015) 333–339.
[29] E. Muchuweni, B.S. Martincigh, V.O. Nyamori, Recent advances in graphene-based materials for dye-sensitized solar cell fabrication, RSC Adv. 10 (72) (2020) 44453–44469.
[30] Q. Wang, L. Qiu, X. Tan, Z. Liu, S. Gao, R. Wang, Amorphous TiO2 granular nanodisks on porous Ti foam for highly effective solar cells and photocatalysts, J. Taiwan Inst. Chem. Eng. 102 (2019) 85–91.
[31] J. Singh, et al., Synthesis, band-gap tuning, structural and optical investigations of Mg doped ZnO nanowires, CrystEngComm 14 (18) (2012) 5898–5904.
[32] M. Khairy, W. Zakaria, Effect of metal-doping of TiO2 nanoparticles on their photocatalytic activities toward removal of organic dyes, Egyptian J. Petrol. 23 (4) (2014) 419–426.
[33] K.M. Reddy, S.V. Manorama, A.R. Reddy, Bandgap studies on anatase titanium dioxide nanoparticles, Mater. Chem. Phys. 78 (1) (2003) 239–245.
[34] L. Wang, et al., Preparation, characterization, and photocatalytic activity of TiO2/ZnO nanocomposites, J. Nanomater. 2013 (2013).
[35] M.N.H. Mia, et al., Influence of Mg content on tailoring optical bandgap of Mg-doped ZnO thin film prepared by sol-gel method, Results Phys. 7 (2017) 2683–2691.
[36] S.P. Lim, et al., Boosting photovoltaic performance of dye-sensitized solar cells using silver nanoparticle-decorated N, S-Co-doped-TiO 2 photoanode, Sci. Rep. 5 (2015), 11922.
[37] J. Zhang, et al., Development of modified N doped TiO 2 photocatalyst with metals, nonmetals and metal oxides, Energy Environ. Sci. 3 (6) (2010) 715–726.
[38] E. Monroy, F. Omnès, F. Calle, Wide-bandgap semiconductor ultraviolet photodetectors, Semicond. Sci. Technol. 18 (4) (2003) R33.
[39] S.J. Kang, et al., Piezoelectric and optical properties of ZnO thin films deposited using various O 2/(Ar+ O 2) gas ratios, J. Mater. Sci. Mater. Electron. 18 (6) (2007) 647–653.
[40] S. Chuhadiya, et al., Thermal annealing induced physical properties of ZnSe thin films for buffer layer in solar cells, Phys. E Low-dimens. Syst. Nanostruct. 117 (2020), 113845.
[41] A.-S. Gadallah, M. El-Nahass, Structural, optical constants and photoluminescence of ZnO thin films grown by Sol-Gel spin coating, Adv. Condens. Matter Phys. 2013 (2013).
[42] J. Tauc, Amorphous and Liquid Semiconductors, Springer Science & Business Media, 2012.
[43] C. Aydin, Synthesis of Pd: ZnO nanofibers and their optical characterization dependent on modified morphological properties, J. Alloys Compd. 777 (2019) 145–151.
[44] M. Khan, et al., Enhancing the efficiency of dye sensitized solar cells by using anatase and brookite mixed phases of TiO2, J. Nanoelectron. Optoelectron. 14 (11) (2019) 1582–1588.
[45] S. Singh, A. Singh, N. Kaur, Efficiency investigations of organic/inorganic hybrid ZnO nanoparticles based dye-sensitized solar cells, J. Mater. 2016 (2016).
[46] M. Khanmirzaei, S. Ramesh, K. Ramesh, Effect of 1-hexyl-3-methylimidazolium iodide ionic liquid on ionic conductivity and energy conversion efficiency of solid polymer electrolyte-based nano-crystalline dye-sensitized solar cells, J. Nanosci. Nanotechnol. 20 (4) (2020) 2423–2429.
[47] N. Mariotti, et al., Recent advances in eco-friendly and cost-effective materials towards sustainable dye-sensitized solar cells, Green Chem. (2020).
[48] P. Christopher, D.B. Ingram, S. Linic, Enhancing photochemical activity of semiconductor nanoparticles with optically active Ag nanostructures: photochemistry mediated by Ag surface plasmons, J. Phys. Chem. C 114 (19) (2010) 9173–9177.
[49] B. Lee, et al., All-solid-state dye-sensitized solar cells with high efficiency, Nature 485 (7399) (2012) 486–489.
[50] J. Xu, et al., Preparation of brookite TiO 2 nanoparticles with small sizes and the improved photovoltaic performance of brookite-based dye-sensitized solar cells, Nanoscale 8 (44) (2016) 18771–18781.
[51] Z. Xiang, et al., Improving energy conversion efficiency of dye-sensitized solar cells by modifying TiO2 photoanodes with nitrogen-reduced graphene oxide, ACS Sustain. Chem. Eng. 2 (5) (2014) 1234–1240.
[52] J.H. Yang, et al., Characteristics of the dye-sensitized solar cells using TiO2 nanotubes treated with TiCl4, Materials 7 (5) (2014) 3522–3532.
[53] G. Zhang, M. Liu, Effect of particle size and dopant on properties of SnO2-based gas sensors, Sensor. Actuator. B Chem. 69 (1–2) (2000) 144–152.
[54] L. Patle, A. Chaudhari, Performance of DSSC with Cu Doped TiO2 electrode prepared by dip coating technique, Int. J. Sci. Eng. Res. 7 (2016) 1004–1009.

[55] X. Lü, et al., Improved-performance dye-sensitized solar cells using Nb-doped TiO2 electrodes: efficient electron injection and transfer, Adv. Funct. Mater. 20 (3) (2010) 509–515.
[56] J. Liu, et al., Photovoltaic performance improvement of dye-sensitized solar cells based on tantalum-doped TiO2 thin films, Electrochim. Acta 56 (1) (2010) 396–400.
[57] A. Caglar, N. Aktas, H. Kivrak, Tailoring cadmium composition on titanium dioxide to achieve enhanced photocatalytic glucose fuel cell anode performance, ACS Appl. Energy Mater. 4 (11) (2021) 12298–12309.
[58] K.K. Wong, A. Ng, X.Y. Chen, Y.H. Ng, Y.H. Leung, K.H. Ho, D.L. Phillips, Effect of ZnO nanoparticle properties on dye-sensitized solar cell performance, ACS Appl. Mater. Interfaces 4 (3) (2012) 1254–1261.
[59] R. Sharma, A. Sarkar, R. Jha, A. Kumar Sharma, D. Sharma, Sol-gel–mediated synthesis of TiO2 nanocrystals: structural, optical, and electrochemical properties, Int. J. Appl. Ceram. Technol. 17 (3) (2020) 1400–1409.